SERBIAN JOURNAL OF ELECTRICAL ENGINEERING
Vol. 6, No. 1, May 2009, 15-31
UDK: 621.45.01; 629.7

Analytical and Numerical Calculation of Magnetic Field Distribution in the Slotted Air-Gap of Tangential Surface Permanent-Magnet Motors

Kamel Boughrara[1], Rachid Ibtiouen[1], Omar Touhami[1], Damir Zarko[2]

Abstract: This paper deals with the analytical and numerical analysis of the flux density distribution in the slotted air gap of permanent magnet motors with surface mounted tangentially magnetized permanent magnets. Two methods for magnetostatic field calculations are developed. The first one is an analytical method in which the effect of stator slots is taken into account by modulating the magnetic field distribution by the complex relative air gap permeance. The second one is a numerical method using 2-D finite element analysis with consideration of Dirichlet and anti-periodicity (periodicity) boundary conditions and Lagrange Multipliers for simulation of movement. The results obtained by the analytical method are compared to the results of finite-element analysis.

Keywords: Finite element method, Conformal mapping, Air-gap permeance, Cogging torque, Permanent-magnet motors.

1 Introduction

The torque in permanenet-magnet motors consist of three basic components: reluctance torque, cogging torque and electromagnetic torque. In order to predict them precisely, it is necessary to analyze both radial and tangential components of the flux density.

Many earlier works have used the analytical models of slotting only for radially or parallelly magnetized surface permanent-magnet motors [1-8]. In the developed analytical method presented in this paper, the field distribution in tangentially magnetized permanent-magnet motors is obtained by solving the equations in polar coordinate system with initial assumption of a smooth stator surface. The effect of slotting is then taken into account by modulating the magnetic field distribution in the smooth air gap by complex relative air gap permeance calculated from conformal transformation of the slot geometry [2-3].

[1]Ecole Nationale Polytechnique (ENP), Algiers, 10, av. Pasteur, El Harrach, BP182, 16200, Algeria;
E-mail: boughrarakamel@yahoo.fr
[2]Faculty of Electrical Engineering and Computing, Department of Electrical Machines,
Drives and Automation, University of Zagreb, HR-10000, Croatia.

The field is calculated numerically using 2-D finite element analysis with Lagrange multipliers used for simulation of movement and with consideration of Dirichlet and anti-periodicity boundary conditions [9]. The objective of the numerical study is to verify the accuracy of the analytical model in predicting the flux density distribution. In order to insure the reliability of results from a finite element calculation, the density of the mesh in the air-gap region and near the tooth tips is doubled.

In this paper we present an improved analytical and numerical method for calculation of magnetic field in tangential surface-mounted permanent-magnet motor from which cogging torque, electromagnetic torque and back-emf waveforms can be calculated as well.

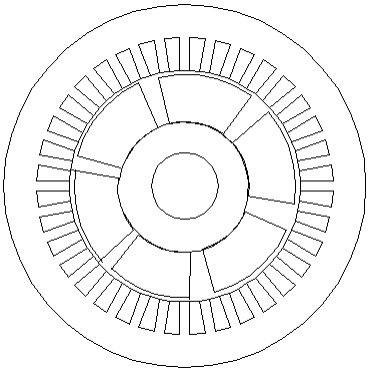

Fig. 1 – *Studied tangential surface permanent-magnet motor*.

2 Analytical Study Model

The studied motor is analyzed at no-load operating conditions. In order to obtain the air-gap field distribution, the following assumptions are used:

- Two-dimensional study model,
- The magnetization M of permanent magnets has a tangential direction and the permeability of magnets equals the permeability of vacuum $\mu_0 = 4\pi \cdot 10^{-7}$ Vs/Am,
- Stator and rotor core steel has infinite permeability,
- The conductivity of all regions is assumed to be zero, i.e., eddy current effects are ignored, and
- The actual slot shape is simplified to a rectangular shape and the width of the rectangular slot equals the width of the actual slot opening.

In these conditions, the magnet is replaced by a continuous and isotropic region having the permeability of vacuum (μ_0).

A. *Field Distribution on a Smooth Stator Surface*

Because of periodicity, the model needs to cover only one pole pitch of the slotless machine. In the studied structure shown in Fig. 1, one point is located by r and θ and the inter-polar axis is defined as the axis of origin ($\theta = 0$).

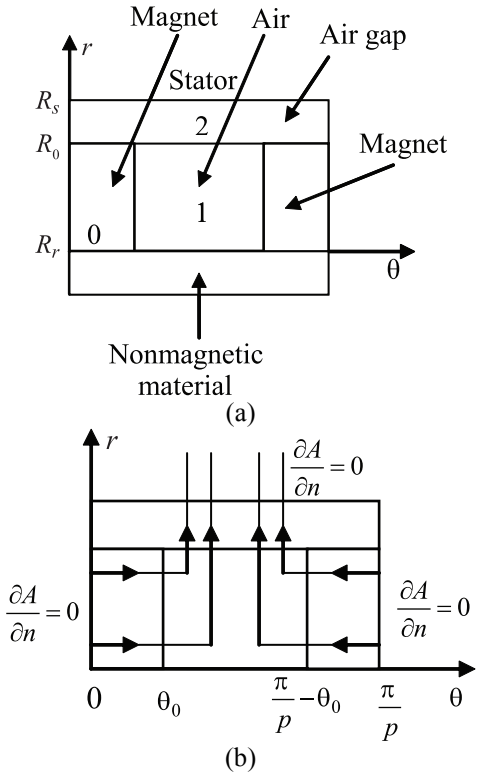

Fig. 2 – *Studied domain*.

For a two-dimensional problem, the magnetic vector potential $\boldsymbol{A}$ will only have a component in the *z*-direction. The flux density is deduced from

$$B_r = \frac{\partial A}{r\partial\theta} \quad \text{and} \quad B_\theta = -\frac{\partial A}{\partial r}. \tag{1}$$

The magnetization $\boldsymbol{M}$ of permanent magnets is defined by $\boldsymbol{B} = \mu_0(\boldsymbol{H} + \boldsymbol{M})$. The actual magnet volume is realized by small elementary bars. The magnetization is considered to be tangential and rigid so that $\operatorname{rot} \boldsymbol{M} = 0$. The magnetomotive force, which is distributed over the magnet height, is replaced by a series of infinitesimal current sheets $\boldsymbol{J}_s$ located in the air, on both sides along the magnet height. If $\operatorname{div} \boldsymbol{M} = 0$ is adopted, then M is proportional to $1/r$ and we obtain the periodic distribution of the equivalent superficial current densities:

$$J_s = \pm M \frac{r_m}{r}, \tag{2}$$

where M is the vector of magnetization at the radius $r_m = \left(R_0 + R_r\right)/2$, R_r is the inner rotor radius and R_0 is the outer rotor radius (Fig. 2a).

Two zones are considered: zone (1) which contains the magnets $\left(R_r < r < R_0\right)$ and zone (2) above the magnets $\left(R_0 < r < R_s\right)$, where R_s is the inner stator radius.

The equivalent superficial current density is given by (2) and represented by a Fourier series as follows:

$$J_s(r,\theta) = \sum_k J_{sk}(r)\cos((2k+1)p\theta), \tag{3}$$

where

$$J_{sk}(r) = \frac{4}{\pi}\frac{M r_m}{r\left(2k+1\right)}\sin((2k+1)p\theta_0) \tag{4}$$

and θ_0 is one half of the angular span of magnets.

In the zones (1) and (2) the equations for vector potential are

$$\Delta \boldsymbol{A}(r,\theta) = 0, \tag{5}$$

with

$$A(r,\theta) = \sum_k \alpha_k(r)\cos((2k+1)p\theta), \tag{6}$$

one has

$$\frac{\mathrm{d}^2\alpha_k(r)}{\mathrm{d}r^2} + \frac{\mathrm{d}\alpha_k(r)}{r\,\mathrm{d}r} - \left[\frac{(2k+1)p}{r}\right]^2 \alpha_k(r) = 0, \tag{7}$$

with $\frac{\mathrm{d}\alpha_k(r)}{\mathrm{d}r} = 0$ at $r = R_s$ (Fig. 2b), $\alpha_k(r)$ is

$$\alpha_k(r) = a_k\left[\left(\frac{r}{R_s}\right)^{(2k+1)p} + \left(\frac{R_s}{r}\right)^{(2k+1)p}\right]. \tag{8}$$

The magnetic vector potential due to superficial current density at $r = R_r$ satisfies the equation $-\frac{\partial A}{\partial r} = \mu_0 J_s(R_r,\theta)$. Therefore

$$a_k = \frac{4p}{\pi} M r_m \frac{\sin\left(\left(2k+1\right)p\theta_0\right)}{\left(\left(2k+1\right)p\right)^2 \sinh\left(\left(2k+1\right)\gamma\right)}, \tag{9}$$

with $\left(\frac{R_r}{R_s}\right)^p = \mathrm{e}^{\gamma}$, in order to get the magnetic vector potential in the zones (1) and (2) due to superficial current density at $r = R_0$ we have $\frac{\mathrm{d}\alpha_{1k}(r)}{\mathrm{d}r} = 0$ for $r = R_r$ and $\frac{\mathrm{d}\alpha_{2k}(r)}{\mathrm{d}r} = 0$ for $r = R_s$. Therefore, in the zones (1) and (2) one has

$$\alpha_{1k}(r) = b_k \left[\left(\frac{r}{R_r}\right)^{(2k+1)p} + \left(\frac{R_r}{r}\right)^{(2k+1)p} \right], \tag{10}$$

$$\alpha_{2k}(r) = c_k \left[\left(\frac{r}{R_s}\right)^{(2k+1)p} + \left(\frac{R_s}{r}\right)^{(2k+1)p} \right]. \tag{11}$$

For $r = R_0$ one has $A_1(r,\theta) = A_2(r,\theta)$ and

$$\frac{\partial A_1(r,\theta)}{\partial r} - \frac{\partial A_2(r,\theta)}{\partial r} = \mu_0 J_s(r,\theta).$$

The expressions for the constants b_k and c_k are

$$b_k = \frac{\cosh\left((2k+1)\alpha\right)}{\sinh\left((2k+1)(\alpha+\beta)\right)} \frac{4pMr_m}{2\pi} \frac{\sin\left((2k+1)p\theta_0\right)}{\left((2k+1)p\right)^2}, \tag{12}$$

$$c_k = \frac{\cosh\left((2k+1)\beta\right)}{\sinh\left((2k+1)(\alpha+\beta)\right)} \frac{4pMr_m}{2\pi} \frac{\sin\left((2k+1)p\theta_0\right)}{\left((2k+1)p\right)^2}, \tag{13}$$

with $\left(\frac{R_s}{R_0}\right)^p = \mathrm{e}^{\alpha}$ and $\left(\frac{R_0}{R_r}\right)^p = \mathrm{e}^{\beta}$ the total vector potential in the zones (1) and (2) is given by

$$\begin{aligned} A_1(r,\theta) = \sum_k \Bigg\{ & a_k \left[\left(\frac{r}{R_s}\right)^{(2k+1)p} + \left(\frac{R_s}{r}\right)^{(2k+1)p} \right] + \\ & + b_k \left[\left(\frac{r}{R_r}\right)^{(2k+1)p} + \left(\frac{R_r}{r}\right)^{(2k+1)p} \right] + \cos\left((2k+1)p\theta\right) \Bigg\}, \end{aligned} \tag{14}$$

$$A_2(r,\theta)=\sum_k\left\{a_k\left[\left(\frac{r}{R_s}\right)^{(2k+1)p}+\left(\frac{R_s}{r}\right)^{(2k+1)p}\right]+\right.$$
$$\left.+c_k\left[\left(\frac{r}{R_s}\right)^{(2k+1)p}+\left(\frac{R_s}{r}\right)^{(2k+1)p}\right]+\cos\left((2k+1)p\theta\right)\right\}. \tag{15}$$

The radial and tangential flux density in the zones (1) and (2) is then

$$B_{1r}(r,\theta)=-\frac{p}{r}\sum_k(2k+1)\left\{a_k\left[\left(\frac{r}{R_s}\right)^{(2k+1)p}+\left(\frac{R_s}{r}\right)^{(2k+1)p}\right]+\right.$$
$$\left.+b_k\left[\left(\frac{r}{R_r}\right)^{(2k+1)p}+\left(\frac{R_r}{r}\right)^{(2k+1)p}\right]+\sin\left((2k+1)p\theta\right)\right\}, \tag{16}$$

$$B_{1\theta}(r,\theta)=-\frac{p}{r}\sum_k(2k+1)\left\{a_k\left[\left(\frac{r}{R_s}\right)^{(2k+1)p}-\left(\frac{R_s}{r}\right)^{(2k+1)p}\right]+\right.$$
$$\left.+b_k\left[\left(\frac{r}{R_r}\right)^{(2k+1)p}-\left(\frac{R_r}{r}\right)^{(2k+1)p}\right]+\cos\left((2k+1)p\theta\right)\right\}, \tag{17}$$

$$B_{2r}(r,\theta)=-\frac{p}{r}\sum_k(2k+1)\left\{a_k\left[\left(\frac{r}{R_s}\right)^{(2k+1)p}+\left(\frac{R_s}{r}\right)^{(2k+1)p}\right]+\right.$$
$$\left.+c_k\left[\left(\frac{r}{R_s}\right)^{(2k+1)p}+\left(\frac{R_s}{r}\right)^{(2k+1)p}\right]+\sin\left((2k+1)p\theta\right)\right\}, \tag{18}$$

$$B_{2\theta}(r,\theta)=-\frac{p}{r}\sum_k(2k+1)\left\{a_k\left[\left(\frac{r}{R_s}\right)^{(2k+1)p}-\left(\frac{R_s}{r}\right)^{(2k+1)p}\right]+\right.$$
$$\left.+c_k\left[\left(\frac{r}{R_s}\right)^{(2k+1)p}-\left(\frac{R_s}{r}\right)^{(2k+1)p}\right]+\cos\left((2k+1)p\theta\right)\right\}. \tag{19}$$

B. *Model of Slotting Effect in Flux Density*

The effect of slotting was modeled in [1] by using relative air gap permeance obtained from a real conformal function which is able take into account only the effect of slotting in the radial flux density by multiplying the field distribution in the slotless air gap with this permeance. This field solution is reasonably accurate if the field is calculated at the radius far enough from the stator bore so that the influence of the tooth tips on the flux density waveform is not significant.

The method presented in this paper and developed by Zarko [2,3] in the case of permanent magnet motors with slotted airgap and with radial or parallel magnetization provides a more complete analytical field solution than developed by Zhu [1] and used in several other papers as well [4-8]. This method allows one to calculate accurately both radial and tangential components of the air gap flux density. It uses the complex nature of the conformal transformation more extensively and defines the relative air gap permeance λ as a complex number. This method, presented in detail in [2], has been used in this paper to calculate the flux density in motors with tangential surface mounted permanent magnets. Therefore, in this paper only the final solution is given. The basic principle of the method is to transform the geometric shape in Fig. 3 into a slotless airgap in which the field solution can be easily found (Fig. 4).

The flux density in the slotted air gap B_s in the S plane is

$$B_s = B_k * \left(\frac{\partial k}{\partial s} \right)^* , \tag{20}$$

where B_k is the field solution in the slotless air gap (K plane) given as $B_k = B_r + \mathrm{j}B_\theta$ with $B_r = B_{1r}$ or $B_r = B_{2r}$ and $B_\theta = B_{1\theta}$ or $B_\theta = B_{2\theta}$. The complex permeance is defined by the following equations:

$$\frac{\partial k}{\partial s} = \lambda = \frac{k}{s} \frac{w-1}{(w-a)^{\frac{1}{2}} (w-b)^{\frac{1}{2}}} , \tag{21}$$

$$k = R_s \, \mathrm{e}^{\mathrm{j}\left(\frac{g'}{\pi} \ln w + \frac{\theta_s}{2} \right)} , \tag{22}$$

$$z = \ln(s) \quad \text{with} \quad s = r \, \mathrm{e}^{\mathrm{j}\theta} , \tag{23}$$

$$z = \mathrm{j} \frac{g'}{\pi} \left[\ln \left| \frac{1+p}{1-p} \right| - \ln \left| \frac{b+p}{b-p} \right| - 2 \frac{b-1}{\sqrt{b}} \tan^{-1} \frac{p}{\sqrt{b}} \right] + C , \tag{24}$$

$$p = \sqrt{\frac{w-b}{w-a}}, \quad C = \ln R_s + \mathrm{j}\theta_2, \quad g' = \ln\left(\frac{R_s}{R_r}\right),$$

$$b = \left[\frac{b_0'}{2g'} + \sqrt{\left(\frac{b_0'}{2g'}\right)^2 + 1}\right]^2, \quad a = \frac{1}{b}, \quad b_0' = \theta_2 - \theta_1$$

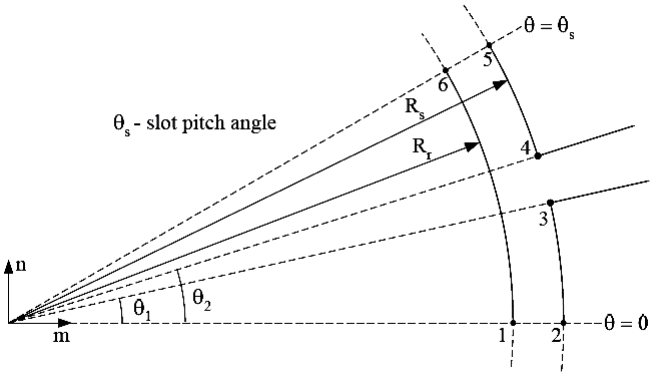

Fig. 3 – *Single infinitely deep slot opening in the S plane.*

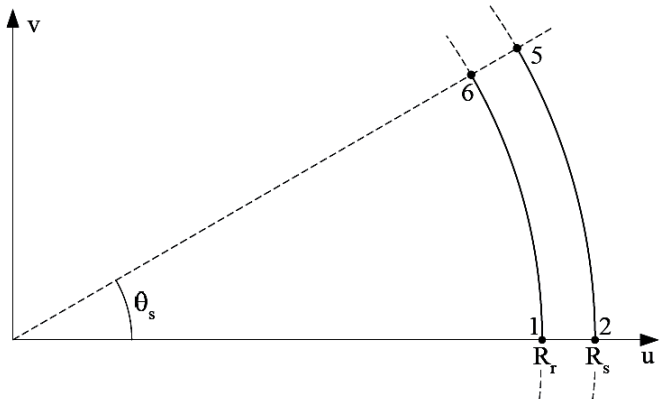

Fig. 4 – *Slot opening in the K plane.*

The value of s is known since it is a coordinate in the slotted air gap where the field is to be calculated. If it is required to calculate the flux density at a certain geometric point in the slotted air gap, then the value of w which corresponds to that point can be calculated from $z = f(w)$, where f is a nonlinear complex function of w. An iterative techniques is required to solve this nonlinear equation and find the value of w for the given z.

Since λ is a complex number, it can be written in the form $\lambda = \lambda_a + \mathrm{j}\lambda_b$. The real and imaginary part can be written in the form

$$\lambda_a = \lambda_0 + \sum_{n=1}^{N_\lambda} \lambda_{an} \cos\left(nQ_s\theta\right), \tag{25}$$

$$\lambda_b = \sum_{n=1}^{N_\lambda} \lambda_{bn} \sin\left(nQ_s\theta\right), \tag{26}$$

where Q_s is the number of slots and N_λ is the maximum order of the Fourier coefficients. The Fourier coefficients λ_{an} and λ_{bn} are calculated from the waveforms of λ_a and λ_b using discrete Fourier transform (FFT).

With $B_s = B_{sr} + \mathrm{j}B_{s\theta}$, the radial and tangential components of the flux density in the slotted air gap are then

$$B_{sr} = \mathrm{Re}\left(B_k\lambda^*\right) = B_r\lambda_a + B_\theta\lambda_b, \tag{27}$$

$$B_{s\theta} = \mathrm{Im}\left(B_k\lambda^*\right) = B_\theta\lambda_a - B_r\lambda_b. \tag{28}$$

C. *Analytical Calculation of Cogging Torque*

For cogging torque calculation we have adopted an alternative approach to the integrating of the magnetic stress on the closed surface around the body. It is based on integration of the magnetic stress vector along the slot sides. The torque per slot is given by [2], [3]

$$T_{slot} = \frac{l_a}{2\mu_0}\int_a^b |B_k|^2 \left|\frac{g'}{\pi}k^2\frac{w-1}{w(w-a)^{\frac{1}{2}}(w-b)^{\frac{1}{2}}}\right| \mathrm{d}w, \tag{29}$$

where $\theta = \frac{g'}{\pi}\ln w + \frac{\theta_s}{2}$, and w, a, b, k, g', B_k are obtained from equations (22), (23) and (24) respectively. The total cogging torque is equal to

$$T_c = \sum_{k=1}^{Q_s} T_{slot}. \tag{30}$$

For practical implementation on the digital computer the integration of (29) needs to be performed from $a+\varepsilon$ to $b-\varepsilon$, where ε is a small number relative to a and b. The reason for using ε is to avoid division by zero.

3 Numerical Study Model

In order to provide comparison of numerical and analytical study models (Fig. 1), the same initial assumptions are made in both models. In these conditions the magnet is replaced by a continuous and isotropic region having the same permeability as air (μ_0). The magnetomotive force of the magnet,

which is distributed over the magnet height, is replaced by a series of infinitesimal current sheets j_s located in the air on both sides along the magnet height. The current sheet is defined by

$$j_s = \pm \frac{M}{\mu_0}. \tag{31}$$

The work is done in a transverse section using a single component magnetic vector potential (MVP) as a state variable. Since only steady state is considered, the rotational speed of the rotor (Ω) is not a function of time. One can define the rotor region Ω_r and the stator region Ω_s each being associated with a frame of reference to which they are fixed. In order to separate these two reference frames the following notation is adopted: x (x') indicates the position in the frame of reference of the stator (the rotor) anywhere in the $R2$ plane. The relationship between x and x' is symbolically noted by

$$x = x' + \Omega t \quad \Leftrightarrow \quad \left\{ \left[x = \begin{pmatrix} r \\ \theta \end{pmatrix} \right] = \left[x' + \Omega t = \begin{pmatrix} r' \\ \theta' \end{pmatrix} + \begin{pmatrix} 0 \\ \Omega t \end{pmatrix} \right] \right\}. \tag{32}$$

The Maxwell's equation in the form of MVP are written as follows:

$$\nabla \left(\frac{1}{\mu_s} \nabla a_s \right) + j_s = 0, \tag{33}$$

$$\nabla \left(\frac{1}{\mu_r} \nabla a_r \right) + j_s = 0, \tag{34}$$

where nabla operator ∇ is referenced to its variables (x or x'), j_s is the current density in the stator, μ_s (μ_r) is the magnetic permeability, which is a function of the position x in Ω_s and x' in Ω_r.

In the context of finite element method [9], (33) and (34) can be written in the matrix form (Fig. 5):

$$\{S_r\}[A_r] = [F_r] \quad \text{For the rotor,}$$

$$\{S_s\}[A_s] = [F_s] \quad \text{For the stator,}$$

where $\{S_s\}$ and $\{S_r\}$ are the stiffness matrices, and $[F_r]$ and $[F_s]$ are the vectors. In order to use (33) and (34) the connection between a_r and a_s must be established. If Ω_r and Ω_s have a common boundary Γ (Fig. 5), then the connection would be

$$a_s(\theta,t) = a_r(\theta',t) \quad \text{on } \Gamma, \tag{35}$$

$$\frac{1}{\mu_s}\frac{\partial a_s(\theta,t))}{\partial n} = \frac{1}{\mu_r}\frac{\partial a_r(\theta',t)}{\partial n} \text{ on } \Gamma, \tag{36}$$

where n is a normal field on Γ, oriented outward from Ω_r. Equations (35) and (36) ensure the continuity of the MVP and its weighted normal derivative.

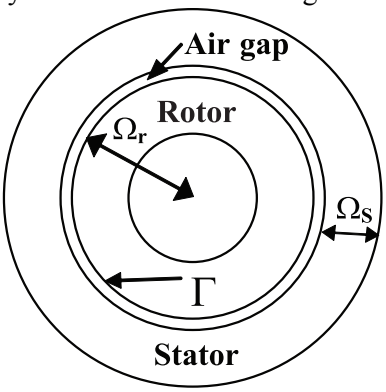

Fig. 5 – *Simplified geometry of the motor*
(*the air gap is zoomed and the slots are not represented*).

A. *Coupling of Stator and Rotor*

Equation (35) allows the coupling between rotor and stator without any need for remeshing (see Fig. 5) by introducing a Lagrange multiplier [9]. The matrix form of the finite element problem with the coupling is

$$\begin{bmatrix} S_s & 0 & I^t \\ 0 & S_r & C^t \\ I & C & 0 \end{bmatrix} \begin{Bmatrix} A_s \\ A_r \\ \lambda \end{Bmatrix} = \begin{Bmatrix} F_s \\ F_r \\ 0 \end{Bmatrix}. \tag{37}$$

For movement with multiple number of angular meshing the matrix $[C]$ consists of -1, 1 and 0. In the case of non-regular angle of rotation, each node of rotor in Γ is coupled to the nodes in the adjacent element by applying the given constraints on the interfaces [9] in the system of equations (37) according to

$$A_r^i = \frac{z_i - z_k}{z_j - z_k} A_s^j + \frac{z_i - z_j}{z_k - z_j} A_s^k, \tag{38}$$

where z_i, z_j and z_k are the angles of nodes i, j and k respectively. Equation (38) is compatible with the usual shape function of the Finite element method evaluated at each node of the interface Γ.

B. *Anti-periodicity Conditions*

The anti-periodicity condition in Ω_r and Ω_s has been introduced in the same manner as

$$\{A_{sa1}\} = [C_{sa}]\{A_{sa2}\}, \tag{39}$$

$$\{A_{ra1}\} = [C_{ra}]\{A_{ra2}\}, \tag{40}$$

where $\{A_{sa1}\}$, $\{A_{sa2}\}$, $\{A_{ra1}\}$ and $\{A_{ra2}\}$ are magnetic potentials of anti-periodic nodes of stator and rotor. The matrices $[C_{sa}]$ and $[C_{ra}]$ contain the combinations of numbers 1 and 0.

C. *Dirichlet Conditions*

For Dirichlet condition the equations $\{A_{sd}\} = 0$ and $\{A_{rd}\} = 0$ are introduced in the global stiffness matrix as

$$[C_{rd}]\{A_{rd}\} = [S] \quad \text{for the rotor space,} \tag{41}$$

$$[C_{sd}]\{A_{sd}\} = [S] \quad \text{for the stator space,} \tag{42}$$

where $\{S\} = 0$ and $[C_{rd}]$, $[C_{sd}]$ contain the combinations of numbers 1 and 0.

D. *Cogging Torque Numerical Calculation*

The global stiffness matrix of the problem is solved by direct method using LU factorization. The flux density is then calculated using (1) and the cogging torque waveform is obtained by solving the following integral equation [9]:

$$T_c = \frac{2pl_a r^2}{\mu_0} \int_0^{\frac{\pi}{p}} B_r B_\theta \, \mathrm{d}\theta, \tag{43}$$

where l_a is the stack length, p is the number of pair poles of the machine, r is the radius of the integration surface, B_r and B_θ are the radial and tangential components of the flux density at radius r.

4 Results and Discussions

The dimensions of the six pole machine which is used as an example are:

Rotor outer radius: 44.8 mm,

Stator outer radius: 63 mm,

Stator or rotor axial length: 57 mm,

Stator inner radius: 45 mm,

Magnet depth: 29.8 mm, and

Angular width of magnet: 12 mechanical degrees.

The stator has 3 phases with single-layer winding and 36 slots with mechanical width of 4 degrees. The average remanence of a ferrite permanent magnet is 0.4 T with relative recoil permeability equal to one.

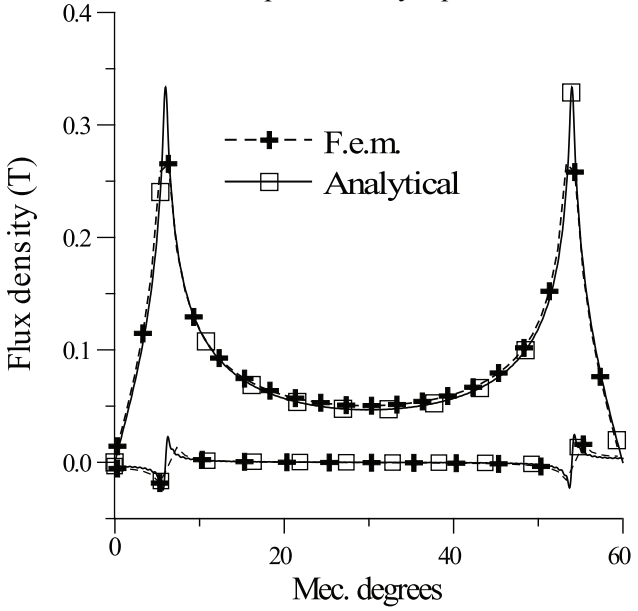

Fig. 6 – *Analytically and numerically calculated radial and tangential flux density at* $r = R_s - g/2$ *in the slotless surface-mounted tangential permanent magnet motor*.

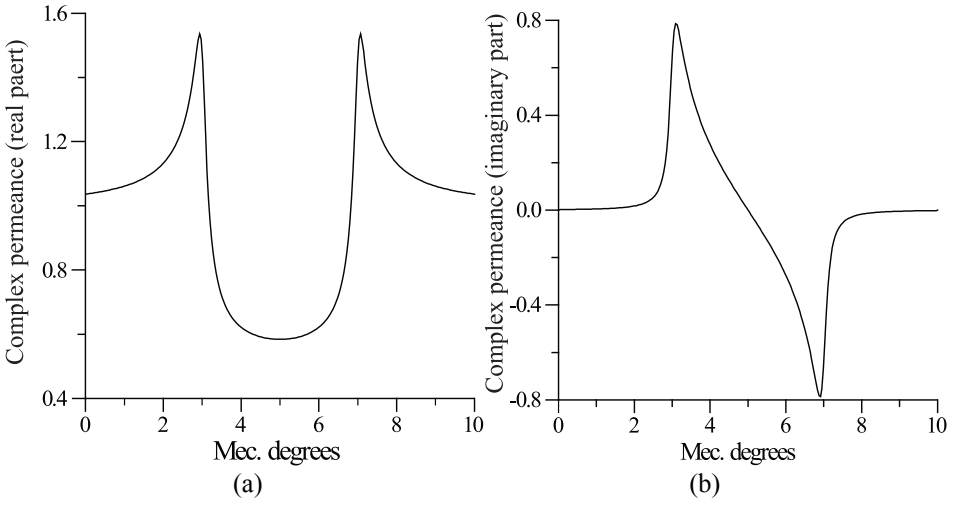

Fig. 7 – *Analytically calculated real* (a) *and imaginary* (b) *parts of the complex relative air-gap permeance at* $r = R_s - g/2$.

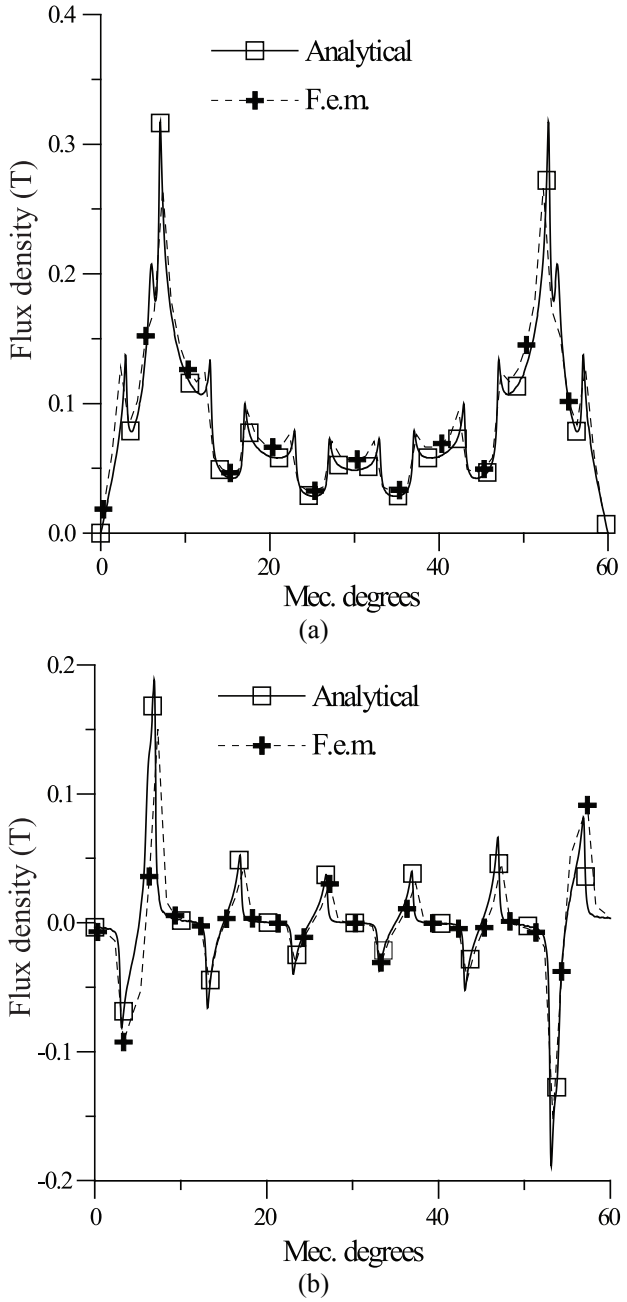

Fig. 8 – *Analytically and numerically calculated radial* (a) *and tangential* (b) *flux density at* $r = R_s - g/2$ *in the slotted surface-mounted tangential permanent-magnet motor.*

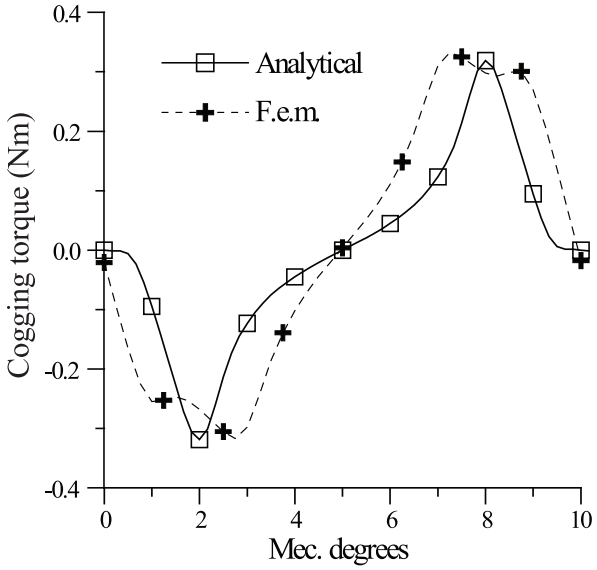

Fig. 9 – *Analytically and numerically calculated cogging torque in the surface-mounted tangential permanent-magnet motor.*

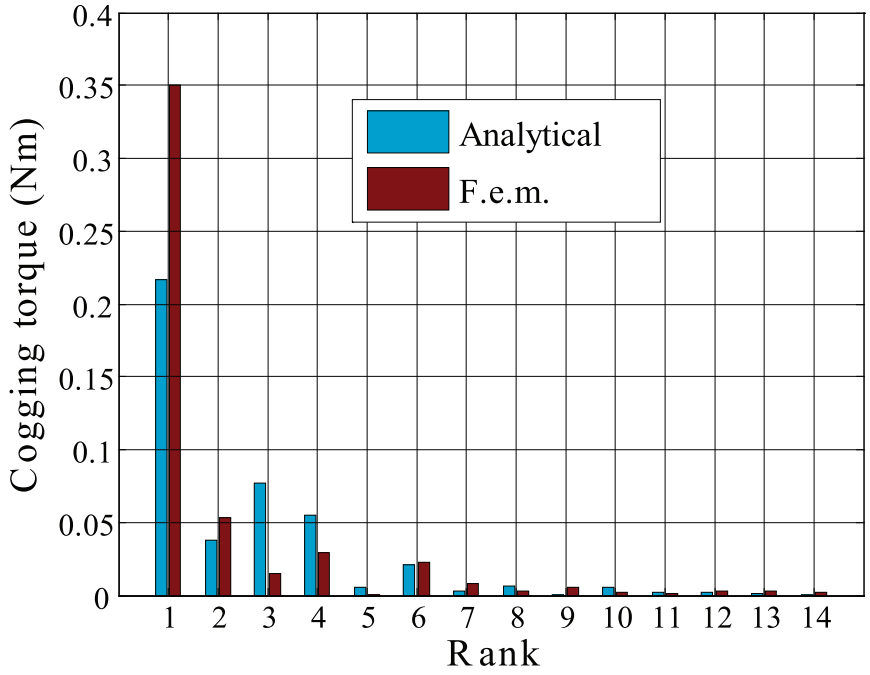

Fig. 10 – *Analytically and numerically calculated cogging torque spectrum in the surface-mounted tangential permanent-magnet motor.*

Fig. 6 shows the distribution of radial and tangential components of flux density due to magnets alone in the slotless motor. The waveforms of the real and imaginary parts of λ calculated at the radius $r = R_s - g/2$ are shown in Fig. 7. They represent one period of the complex permeance distribution which extends one slot pitch. Fig. 8 shows the distribution of radial and tangential flux density due to magnets alone in the slotted motor. Figs. 9 and 10 show the cogging torque waveform and spectrum. The air-gap magnetic field and cogging torque obtained numerically and analytically are in good agreement.

5 Conclusion

This paper describes improved analytical and numerical methods for the analysis of brushless tangential permanent-magnet synchronous motors which take into account the effect of slotting in distribution of both radial and tangential flux density components.

The use of the Lagrange multipliers in the finite element analysis guarantees the stator-rotor coupling and facilitates the introduction of Dirichlet boundary conditions, and periodicity or anti-periodicity boundary conditions as well, while guaranteeing at the same time that condition for maintaining the rigidity of the matrix is satisfied. This approach avoids the equations system to become singular when solved by either numerical direct or iterative methods.

6 References

A. Z.Q. Zhu, D. Howe: Instantaneous Magnetic Field Distribution in Brushless Permanent Magnet DC Motors, Part III: Effect of Stator Slotting, IEEE Transaction on Magnetics, Vol. 29, No. 1, 1993, pp. 143-151.

[1] D. Zarko, D. Ban, T.A. Lipo: Analytical Calculation of Magnetic Field Distribution in the Slotted Air Gap of a Surface Permanent-magnet Motor using Complex Relative Air-gap Permeance, IEEE Transaction on Magnetics, Vol. 42, No. 7, 2006, pp. 1828-1837.

[2] D. Zarko, D. Ban, T.A. Lipo: Analytical Solution for Cogging Torque in Surface Permanent-Magnet Motors using Conformal Mapping, IEEE Transaction on Magnetics, Vol. 44, No. 1, 2008, pp. 52-65.

[3] M. Markovic, M. Jufer, Y. Perriard: Determination of Tooth Cogging Force in a Hard-Disk Brushless DC Motor", IEEE Transaction on Magnetics, Vol. 41, No. 12, 2005, pp. 4421-4426.

[4] M. Markovic, M. Jufer, Y. Perriard: Reducing the Cogging Torque in Brushless DC Motors by using Conformal Mappings, IEEE Transaction on Magnetics, Vol. 40, No. 2, 2004, pp. 451-455.

[5] K.H. Kim, D.J. Sim, J.S. Won:Analysis of Skew Effects on Cogging Torque and BEMF for BLDCM, IEEE Industry Applications Society Annual Meeting, Vol. 1, 1991, pp. 191-197.

[6] X. Wang, Q. Li, S. Wang, Q. Li: Analytical Calculation of Air-gap Magnetic Field Distribution and Instantaneous Characteristics of Brushless DC Motors, IEEE Transaction on Energy Conversion, Vol. 18, No. 3, 2003, pp. 424-432.

[7] A.B. Proca, A. Keyhani, A. El-Antably, W. Lu, M. Dai: Analytical Model for Permanent Magnet Motors with Surface Mounted Magnets, IEEE Transaction on Energy Conversion, Vol. 18, No. 3, 2003, pp. 386-391.

[8] K. Boughrara, R. Ibtiouen, O. Touhami: Numerical Analysis of Brushless Permanent Magnet Motors using Lagrange Multiplier, 31st Annual Conference of IEEE Industrial Electronics Society, 2005, pp. 2575-2578.